PROCEEDINGS OF SCIENCE

Investigating collective effects in small collision systems using PYTHIA8 and EPOS4 simulations

C. D. Brandibur, A. Danu, A. F. Dobrin and A. Manea*

Institute of Space Science – INFLPR Subsidiary,
409 Atomistilor Street, Magurele, Romania

E-mail: alexandru.manea@cern.ch

Studies have yielded strong evidence that a deconfined state of quarks and gluons, the quark–gluon plasma, is created in heavy-ion collisions. This hot and dense matter exhibits almost zero friction and a strong collective behaviour. An unexpected collective behaviour has also been observed in small collision systems whose origin is still not understood.

The second and third order Fourier coefficients are reported from EPOS4 simulations of pp collisions at $\sqrt{s}$ = 13.6 TeV. The second and third harmonic two-particle cumulants, denoted as $c_2\{2\}$ and $c_3\{2\}$, respectively, depend on charged-particle multiplicity and $|\Delta\eta|$ gap placed to suppress the contribution from few-particle correlations. The $c_2\{2\}$ with $|\Delta\eta|$ gap is positive and decreases with multiplicity, while the $c_3\{2\}$ with $|\Delta\eta|$ gap is negative and increases with multiplicity. The second and third harmonic four-particle cumulants are consistent with zero over almost the entire multiplicity range which is expected for Gaussian fluctuations. The second-order Fourier coefficient of $\pi^{\pm}$, $K^{\pm}$, p+$\overline{p}$, Λ+$\overline{\Lambda}$, K^0_S, and Ξ^-+$\overline{\Xi}^+$ obtained using the scalar product method is mass-ordered, being more pronounced when a large $|\Delta\eta|$ gap is employed.

EPS-HEP2023 Conference on High Energy Physics,
21-25 August 2023
Hamburg University, Hamburg, Germany

*Speaker

PoS(EPS-HEP2023)203

1. Introduction

Collisions of heavy ions at relativistic energies exhibit a strong collective behaviour which characterizes the hot and dense medium created in such collision, the quark–gluon plasma (QGP). This collective flow is commonly quantified by the v_n coefficients in a Fourier expansion of the azimuthal distribution of produced particles [1]. The measurements of v_n coefficients compared to hydrodynamic models indicate that the QGP is the most perfect fluid.

An unexpected collective behaviour has also been revealed in proton–proton (pp) and p–Pb collisions at the Large Hadron Collider using measurements of two- and multi-particle azimuthal correlations. A near-side ridge (elongated structure in $\Delta\eta$ at $\Delta\varphi \sim 0$ in the two-particle correlation function versus the difference in azimuth, $\Delta\varphi$, and pseudorapidity, $\Delta\eta$) was discovered in high multiplicity pp and p–Pb collisions [2, 3]. In addition, a characteristic mass ordering of the second order coefficient, v_2, at low transverse momentum (p_{T}) and a grouping of v_2 of mesons and baryons at intermediate p_{T} was observed in measurements of identified hadrons [4]. This is qualitatively similar to the pattern observed in heavy-ion collisions.

In these proceedings, the collective behaviour is investigated using two- and multi-particle azimuthal correlations of inclusive and identified particles in EPOS4 simulations [5] of pp collisions at $\sqrt{s}$ = 13.6 TeV. The EPOS4 model implements a “core-corona" picture in which the soft processes of the interaction follow a hydrodynamic evolution (in the “core" region). The strongly-coupled medium has low shear viscosity and can be modelled by hydrodynamic transport equations. Hard processes like jet production are treated using string dynamics in the “corona" region. Three configurations were used in the simulations: “core+corona" (i.e., primary interactions and hydrodynamics) coupled to a hadronic afterburner, “core+corona" without hadronic afterburner, and “core" only. The results from core+corona with hadronic afterburner are compared with PYTHIA8 calculations [6] taken from Ref. [7].

2. Experimental methods

The second and third order Fourier coefficients are measured using the scalar product method [8] and cumulant technique [9, 10]. The former uses

$$v_n\{\mathrm{SP}\} = \frac{\langle \mathbf{u}_{\mathrm{n,k}} \mathbf{Q}^{*}_{\mathrm{n}} / \mathrm{M} \rangle}{\sqrt{\langle \mathbf{Q}^{\mathrm{a}}_{\mathrm{n}} \mathbf{Q}^{\mathrm{b}*}_{\mathrm{n}} / (\mathrm{M^a M^b}) \rangle}}, \tag{1}$$

where φ_k is the azimuthal angle of the particle of interest (POI) k, $\mathbf{u}_{n,k} = \exp in\varphi_k$ is the unit vector of the particle k, $\mathbf{Q}_n = \sum_l \exp in\varphi_l$ is the event flow vector, M is the event multiplicity, and n represents the order of the Fourier coefficient. The full event is divided into two independent sub-events a and b composed of particles from different pseudorapidity intervals with flow vectors $\mathbf{Q}^a_n$ and $\mathbf{Q}^b_n$ and multiplicities M^a and M^b. The angle brackets denote an average over all particles in all events and * the complex conjugate.

Either $\pi^{\pm}$, $\mathrm{K}^{\pm}$, $\mathrm{p}+\overline{\mathrm{p}}$, $\Lambda+\overline{\Lambda}$, $\mathrm{K}^0_{\mathrm{S}}$, or $\Xi^-+\overline{\Xi}^+$ are taken as POI from a p_{T} interval and correlated with all unidentified charged particles from $0.2 < p_{\mathrm{T}} < 3.0$ GeV/c (reference particles, RPs). In order to reduce the contribution from few-particle correlations called “nonflow" (δ_n), such as those due to resonances and jets, a pseudorapidity gap ($|\Delta\eta| > 1.0$) is introduced between POI and RPs

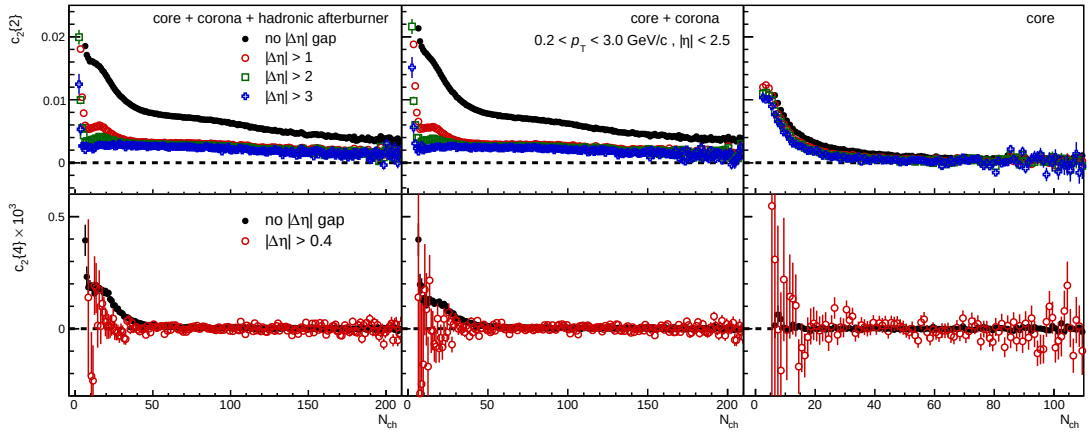

Figure 1: $c_2\{2\}$ (top) and $c_2\{4\}$ (bottom) as a function of charged-particle multiplicity from different EPOS4 configurations of pp collisions at $\sqrt{s} = 13.6$ TeV.

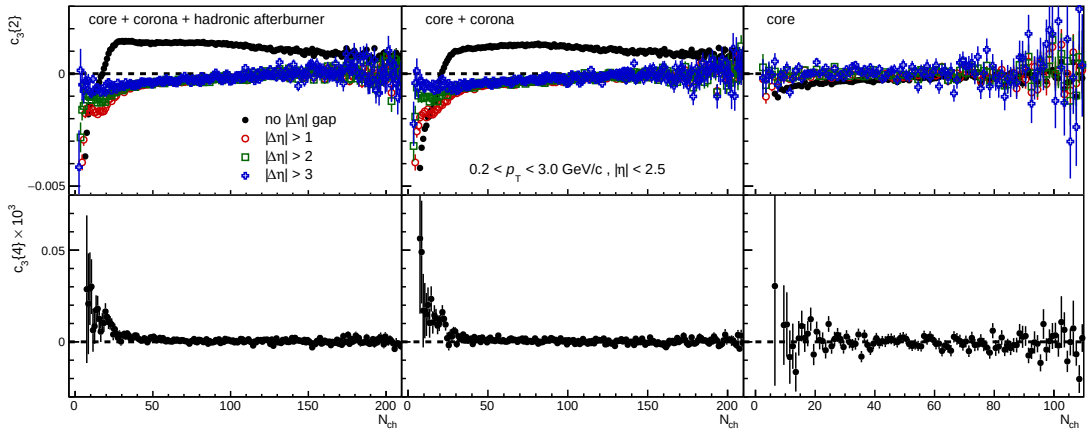

Figure 2: $c_3\{2\}$ (top) and $c_3\{4\}$ (bottom) as a function of charged-particle multiplicity from different EPOS4 configurations of pp collisions at $\sqrt{s} = 13.6$ TeV.

by taking them from $0.5 < \eta < 1.0$ and $-1.0 < \eta < -0.5$, respectively. The nonflow is further suppressed by increasing the $|\Delta\eta|$ gap to $|\Delta\eta| > 2.0$ by choosing the POI from $|\eta| < 1$ and RPs from $-5.0 < \eta < -3.0$.

The two- and four-particle cumulants, which have different responses to nonflow ($\delta_n \propto 1/M^{m-1}$, where m represents the cumulant order) were calculated for unidentified particles with using

$$c_n\{2\} = \langle\langle 2\rangle\rangle \ , \tag{2}$$

$$c_n\{4\} = \langle\langle 4\rangle\rangle - 2 \cdot \langle\langle 2\rangle\rangle^2 \ . \tag{3}$$

3. Results

Figure 1 shows the second order two- ($c_2\{2\}$) and four-particle ($c_2\{4\}$) cumulants of unidentified charged particles as a function of charged-particle multiplicity from EPOS4 simulations

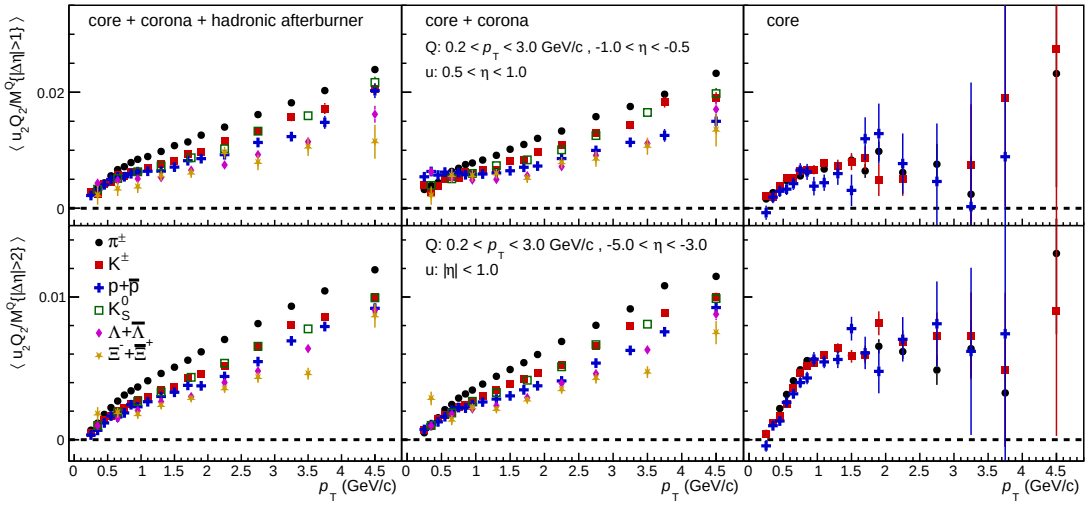

Figure 3: The p_{T}-differential $\langle u_2 Q_2 / M^{Q} \rangle$ of $\pi^{\pm}$, $\mathrm{K}^{\pm}$, $\mathrm{p}+\overline{\mathrm{p}}$, $\Lambda+\overline{\Lambda}$, $\mathrm{K}^{0}_{\mathrm{S}}$, and $\Xi^{-}+\overline{\Xi}^{+}$ for $|\Delta\eta| > 1$ (top) and $|\Delta\eta| > 2$ (bottom) from different EPOS4 configurations of pp collisions at $\sqrt{s} = 13.6$ TeV.

with core+corona (i.e., primary interactions and hydrodynamics) coupled to a hadronic afterburner, core+corona without hadronic afterburner, and core only. The $c_2\{2\}$ decreases with charged-particle multiplicity and $|\Delta\eta|$ gap placed to suppress nonflow. The magnitude of the $c_2\{2\}$ is positive and depends weakly on the $|\Delta\eta|$ gap at high multiplicity for core+corona, while it is consistent with zero for core. The $c_2\{4\}$ is consistent with zero for $\mathrm{N_{ch}} > 50$ for core+corona and over the entire multiplicity range for core. Gaussian fluctuations of the sources would explain this trend. The hadronic afterburner, which involves particles from both core and corona, affects mostly the low-multiplicity region ($\mathrm{N_{ch}} < 40$) since it reduces the low p_{T} yields of baryons due to baryon–antibaryon annihilation. The core configuration shows a weak dependence on the $|\Delta\eta|$ gap since the nonflow contributions come mostly from resonances as jets are not present in this case. In addition, the positive $c_2\{2\}$ at low multiplicity might arise from the conversion of the total available energy into particle flow.

The third harmonic results are presented in Fig. 2. For core+corona, a strong dependence with multiplicity is observed for $c_3\{2\}$ for no $|\Delta\eta|$ gap, reaching negative values for $\mathrm{N_{ch}} < 20$. The $c_3\{2\}$ with $|\Delta\eta|$ gap is negative and increases with multiplicity reaching zero for all $|\Delta\eta|$ gaps at high multiplicity. For core, a weak multiplicity dependence is found for no $|\Delta\eta|$ gap, while $c_3\{2\}$ is consistent with zero for all $|\Delta\eta|$ gaps over the entire multiplicity range. The $c_3\{4\}$ is consistent with zero for all configurations. The nonflow contributions (i.e., events with three jets), which come only from the corona region, are responsible for the observed negative values at low multiplicity, while both corona and core configurations are not able to generate v_3 at high multiplicity.

The p_{T}-differential $\langle u_2 Q_2 / M^{Q} \rangle$ of $\pi^{\pm}$, $\mathrm{K}^{\pm}$, $\mathrm{p}+\overline{\mathrm{p}}$, $\Lambda+\overline{\Lambda}$, $\mathrm{K}^{0}_{\mathrm{S}}$, and $\Xi^{-}+\overline{\Xi}^{+}$ for $|\Delta\eta| > 1$ (top panels) and $|\Delta\eta| > 2$ (bottom panels) gaps is presented for core+corona with and without hadronic afterburner and core in Fig. 3. For core+corona with hadronic afterburner, $\langle u_2 Q_2 / M^{Q} \rangle$ exhibits a mass ordering (i.e., lighter particles have a larger $\langle u_2 Q_2 / M^{Q} \rangle$ than heavier particles at the same p_{T}) which is more pronounced for $|\Delta\eta| > 2$ gap. The mass ordering is broken for both $|\Delta\eta|$ gaps

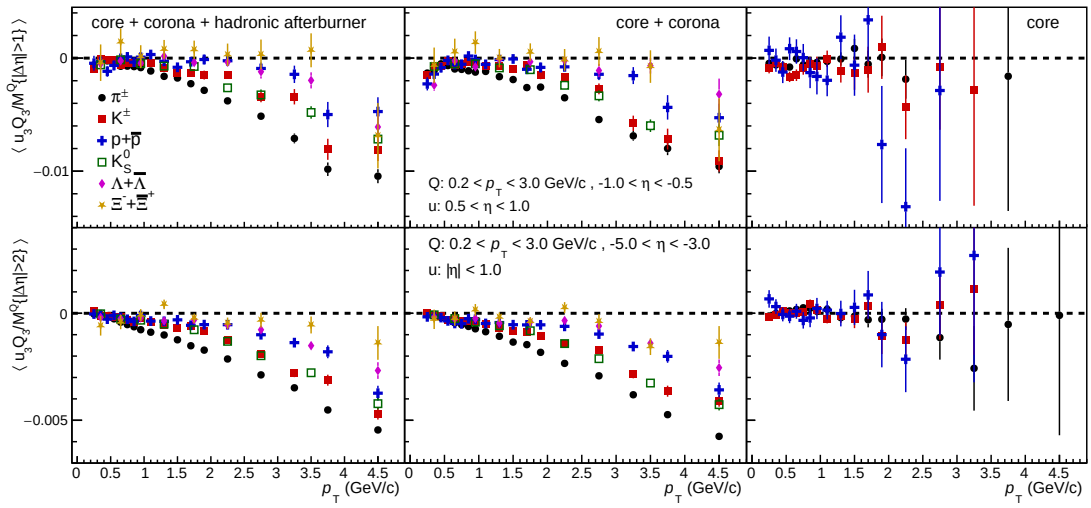

Figure 4: The p_{T}-differential $\langle u_3 Q_3/M^Q\rangle$ of $\pi^{\pm}$, $\mathrm{K}^{\pm}$, $\mathrm{p}+\overline{\mathrm{p}}$, $\Lambda+\overline{\Lambda}$, $\mathrm{K}^0_{\mathrm{S}}$, and $\Xi^-+\overline{\Xi}^+$ for $|\Delta\eta| > 1$ (top) and $|\Delta\eta| > 2$ (bottom) from different EPOS4 configurations of pp collisions at $\sqrt{s}$ = 13.6 TeV.

for $p_{\mathrm{T}} < 1$ GeV/c when the hadronic afterburner is not employed. Therefore, it is important to include the rescattering since it affects mostly baryons making their spectra harder. For the core case, the $\langle u_2 Q_2/M^Q\rangle$ of the different particle species is mass-ordered. No crossing between baryon and meson $\langle u_2 Q_2/M^Q\rangle$ is observed at intermediate p_{T}. In this p_{T} interval the particles are mostly produced from string fragmentation from the corona region. However, a small fraction of high p_{T} partons may escape the core and hadronize in the corona region. The corresponding $\langle u_3 Q_3/M^Q\rangle$ results are shown in Fig. 4. Except for $\Xi^-+\overline{\Xi}^+$, the magnitude of $\langle u_3 Q_3/M^Q\rangle$ for other particle species is negative and decreases with increasing p_{T} for core+corona. This behaviour is in contrast to the core case where the $\pi^{\pm}$, $\mathrm{K}^{\pm}$, and $\mathrm{p}+\overline{\mathrm{p}}$ points are consistent with zero.

Figure 5 shows comparisons of p_{T}-differential $v_2\{2, |\Delta\eta| > 2\}$ of $\pi^{\pm}$, $\mathrm{K}^{\pm}$, $\mathrm{p}+\overline{\mathrm{p}}$, $\Lambda+\overline{\Lambda}$, $\mathrm{K}^0_{\mathrm{S}}$, and $\Xi^-+\overline{\Xi}^+$ from EPOS4 and PYTHIA8 simulations [7]. The configuration of core+corona with hadronic afterburner is used for EPOS4, while rope hadronization [11] and Monash tune [12] are chosen for PYTHIA 8. A good agreement is found for $p_{\mathrm{T}} < 1$ GeV/c, while the $v_2\{2, |\Delta\eta| > 2\}$ from PYTHIA8 is larger than that from EPOS4 for $p_{\mathrm{T}} > 1$ GeV/c.

4. Summary

The EPOS4 model has been used to extract the second and third order Fourier coefficients in pp collisions at $\sqrt{s}$ = 13.6 TeV. The second and third harmonic two-particle cumulants depend on charged-particle multiplicity and $|\Delta\eta|$ gap, while the four-particle cumulants are consistent with zero over almost the entire multiplicity range. The $c_2\{2\}$ with $|\Delta\eta|$ gap is positive and decreases with multiplicity. This behaviour is in contrast to the $c_3\{2\}$ with $|\Delta\eta|$ gap, being negative and increasing with multiplicity. The p_{T}-differential $\langle u_2 Q_2/M^Q\rangle$ of $\pi^{\pm}$, $\mathrm{K}^{\pm}$, $\mathrm{p}+\overline{\mathrm{p}}$, $\Lambda+\overline{\Lambda}$, $\mathrm{K}^0_{\mathrm{S}}$, and $\Xi^-+\overline{\Xi}^+$ is mass-ordered, being more pronounced when a large $|\Delta\eta|$ gap is employed.

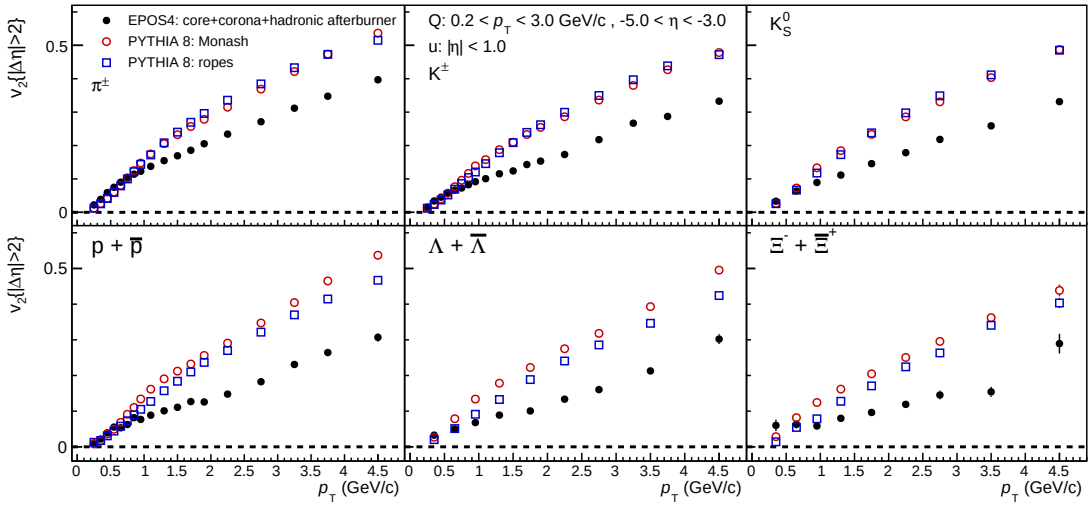

Figure 5: The p_{T}-differential $v_2\{2, |\Delta\eta| > 2\}$ of $\pi^{\pm}$, $\mathrm{K}^{\pm}$, p+$\bar{\mathrm{p}}$, $\Lambda+\overline{\Lambda}$, $\mathrm{K}^0_{\mathrm{S}}$, and $\Xi^-+\overline{\Xi}^+$ from EPOS4 and PYTHIA 8 simulations of pp collisions at $\sqrt{s}$ = 13.6 TeV.

Acknowledgments

This research was supported by a grant of the Ministry of Research, Innovation and Digitization, CNCS – UEFISCDI, project number PN-III-P4-PCE-2021-0390, within PNCDI III.

References

[1] S. Voloshin and Y. Zhang, Z. Phys. C **70** (1996), 665-672.

[2] V. Khachatryan *et al.* [CMS], JHEP **09** (2010), 091.

[3] B. Abelev *et al.* [ALICE], Phys. Lett. B **719** (2013), 29-41.

[4] B. B. Abelev *et al.* [ALICE], Phys. Lett. B **726** (2013), 164-177.

[5] K. Werner, [arXiv:2301.12517 [hep-ph]].

[6] C. Bierlich *et al.*, SciPost Phys. Codebases 8 (2022).

[7] C. D. Brandibur, A. Danu, A. F. Dobrin and A. Manea, these proceedings.

[8] C. Adler *et al.* [STAR], Phys. Rev. C **66** (2002), 034904.

[9] A. Bilandzic, R. Snellings and S. Voloshin, Phys. Rev. C **83** (2011), 044913.

[10] J. Jia, M. Zhou and A. Trzupek, Phys. Rev. C **96** (2017), 034906.

[11] C. Bierlich, G. Gustafson, L. Lönnblad and A. Tarasov, JHEP **03** (2015), 148.

[12] P. Skands, S. Carrazza and J. Rojo, Eur. Phys. J. C **74** (2014), 3024.